The effects of tantalum addition on the microtexture and mechanical behaviour of tungsten for ITER applications

E. Tejado , P.A. Carvalho , A. Munoz , M. Dias , J.B. Correia , U.V. Mardolcar , J.Y. Pastor

A B S T R A C T

Tungsten (W) and its alloys are very promising materials for producing plasma-facing components (PFCs) in the fusion power reactors of the near future, even as a structural part in them. However, whereas the properties of pure tungsten are suitable for a PFC, its structural applications are still limited due to its low toughness, ductile to brittle transition temperature and recrystallization behaviour. Therefore, many efforts have been made to improve its performance by alloying tungsten with other elements.

Hence, in this investigation, the thermo-mechanical performance of two new tungsten-tantalum materials has been evaluated. Materials with W−5wt.%Ta and W−15wt.%Ta were processed by mechanical alloying (MA) and later consolidation by hot isostatic pressing (HIP), with distinct settings for each composition. Thus, it was possible to determine the relationship between the microstructure and the addition of Ta with the macroscopic mechanical properties. These were measured by means of hardness, flexural strength and fracture toughness, in the temperature range of 300−1473 K. The microstructure and the fracture surfaces features of the tested materials were analysed by Field Emission Scanning Electron Microscopy (FESEM).

Keywords:
Tungsten
Tantalum
Fracture toughness
Mechanical properties
High temperature
Nuclear applications

1. Introduction

Nuclear fusion is the least developed of the alternatives to non-renewable energy resources, although it has a high potential for future energy supply since its raw materials are abundant and widely available. However, one of the main obstacles faced for the development of a fusion plant is the designing of materials that will tolerate the harsh radiation environment combined with a strong mechanical stress [1]. Tungsten and tungsten alloys are some of the candidate armour materials for the plasma-facing components of the International Thermonuclear Experimental Reactor and its previous prototype DEMO. For the present reference design, tungsten has been selected as the armour for the divertor, the upper vertical target, the dome, the cassette liner, and for the lower baffle because of its unique resistance to ion and charge-exchange particle erosion in comparison with other materials [2]. For these applications, different tungsten grades (pure, dispersion strengthened and cast alloys) have been considered. However, the mechanical properties of commercially available tungsten are not yet adequate for structural purposes due to the intrinsic brittleness of tungsten at relatively low temperatures, as the ductile−brittle transition (DBTT) occurs in the vicinity of 0.15 T_m, thus limiting the operating temperatures of the reactor. On the other hand, the mechanical properties of W at high temperatures are quite poor, and it exhibits a strong degradation in air due to its linear oxidation.

The approaches towards reducing brittleness of W at low temperatures have not changed since 1975, as reported by W.D. Klopp [3]. These are: i) improvement of purity, ii) maintenance of a fine-

grained or worked structure, iii) incorporation of inert dispersoids and iv) alloying to promote solution softening. Furthermore, it has been found that the addition of certain elements, such as Re, Tc, Ti or Co [4] can improve the ductility of W thereby reducing the DBTT of the alloy. However, some of these elements become activated under neutron irradiation, such as Co or Re; this last one even forms brittle sigma-phase precipitates with the primary products of its nuclear reactions (W–Re–Os) [5].

After rejecting the W–Re alloys for economic and practical reasons, it has been suggested that sintered W heavy alloys (WHA) might meet the requirements of the current designs. In particular, the addition of other refractory metals could lead to an improved tungsten product for divertor applications, as the high melting point, high thermal conductivity and high resistance to sputtering and erosion are shared. Pursuing this approach, Ta could be one of the most auspicious alloying elements [6], since it forms a solid solution with W, does not produce new phases after transmutation and has been widely used to alloy low activation ferritic-martensitic steels in order to reduce their DBTT [7,8].

Several researches have been carried out on the tungsten-rich end of the binary W–Ta system. Therefore this paper is focused on the influence of both microstructure and chemical composition on the fracture behaviour of two tungsten–tantalum alloys as function of temperature. The diverse initial particle sizes and different milling times during manufacturing led to the choice of two materials for study: W–5 wt. %Ta alloy and W–15 wt. %Ta composite. To characterize this, three-point bending and fracture toughness tests were performed in the temperature interval from 300 K to 1473 K (25 °C–1200 °C). Additional studies were carried out in order to determine the thermal diffusivity of the sintered products as well as a basic physical characterization.

2. Experimental details

2.1. Materials and sample preparation

Two tungsten materials containing 5 wt. %Ta (5.12 at %) and approximately 15 wt. %Ta (14.8 wt. % and 15 at %), have been studied. They were both obtained by Hot Isostatic Pressure (HIP) of blended and ball-milled powders. In an effort to better evaluate the influence of the processing parameters on the mechanical performance; those were modified for each material.

Firstly, W–5 wt. %Ta (W–5Ta) was prepared by mixing together elemental powders of pure W (with purity of 99.9%, median particle size 1–5 μm) and Ta (99.9% purity, median particle size less than 2 μm) in a tubular T2F mixer for 4 h. Afterwards, the blended powders were milled for 50 h in a high-energy planetary mill under a high purity Ar atmosphere, in a tungsten carbide (WC) container and using WC balls of ∅ 10 mm with a 4:3 ball-to-powder ratio, as grinding media. Before the consolidation, the alloyed powders were encapsulated in a steel container and degassed for 24 h at 675 K (400 °C) in a vacuum of ~0.2 Pa.

Alternatively, for W–15 wt. % Ta (W–15Ta), W powder (99.95% purity, median particle size 1 μm) was mixed with Ta powder (99.95% purity, median particle size 75 μm) in a Retsch PM400MA planetary ball mill for 4 h under high purity Ar atmosphere mill to obtain the W–15 wt. % Ta composite. Further details of the production and microstructural characterization of W–15Ta can be found in the literature [9].

Afterwards, both materials were deoxidized in an Ar + 10% H_2 atmosphere for 3 h at 1400 K (1100 °C), subsequently canned inside stainless steel cans and degassed at 725 K (450 °C) for 24 h in Ar. The encapsulated compacts were then consolidated by hot isostatic pressing for 2 h at temperatures between 1523 and 1573 K with high purity Ar under 19×10^7 Pa.

Cylindrical billets of 30 mm in diameter and 50 mm in length were obtained after consolidation by HIP. Miniaturized bend specimens (nominal dimensions $1.7 \times 1.7 \times 25$ mm^3) and small discs with a diameter of 15.7 mm and a height of 2 mm were produced by refrigerated electro-discharge machining to comply with the needs of mechanical and thermal-diffusivity testing, respectively.

In addition, pure tungsten was produced as a reference material [10] to serve as basis for comparison with the present study materials.

2.2. Mechanical testing

Materials characterization was performed in an extended high temperature range by means of quasi-static three-point bending (TPB) tests, on smooth and notched specimens. Additionally thermal diffusivity was determined at the expected operation temperatures. Hardness (Vickers and Berkovich indentation), elastic modulus and density by the Archimedes method were measured at 300 K.

Vickers micro-hardness was determined applying a load of 9.8 N for 15 s in an AKASHI MVK-EIII tester. Additionally, nano-indentation to a depth of 1500 nm was performed on the same samples using a standard Berkovich tip, calibrated using fused silica. Average values of hardness and elastic modulus were taken from the unloading curve according to the Oliver and Pharr method [11]. Elastic modulus results where then compared with those obtained by the flexural vibration resonance method (Grindosonic MK4i, J.W. Lemmens, Belgium).

In this investigation, TPB tests were performed with 16 mm span at a constant cross-head travel speed of 100 μm/min, in order to easily control the test process while obtaining accurate recording data. In order to investigate the transition from the ductile to brittle fracture, TPB testing was performed at temperatures between RT and 1273 K in air with a small silicon carbide furnace mounted inside the loading zone of the INSTRON 3369 testing machine used. However, due to material oxidation at temperatures greater than 873 K, testing was also carried out in a vacuum environment with an INSTRON 8501 equipped with a high temperature vacuum furnace (Sigmatest GmbH), up to 1473 K and 2×10^{-4} Pa vacuum pressure. Flexural strength was computed by Euler–Bernoulli equations for slender beams up to failure; however when yield stress was exceeded, 0.2% strength offsets were reported.

Fracture toughness was also determined by means of TPB configuration in the same environments and temperature range. For this purpose, femtosecond laser machined notches were introduced in the samples, obtaining with this method a real crack type as seen in Fig. 1, with no melted layer (or heat affected layer) in the surrounding of the notch. Overall notch lengths were measured under the scanning electron microscope, yielding mean tip radius of 5–20 nm and crack lengths of approximately 250 μm. Finally, fracture toughness was computed from the failure load and the beam section using the stress intensity factor for mode I stress supplied by Guinea et al. [12].

Post-mortem examinations were performed by scanning electron microscopy (SEM). The analysis of the fracture surfaces of samples tested in air was, however, hindered in the samples tested at 873 K and above by the presence of an oxide layer. Additionally, RT samples were mounted and polished to study the microstructure and elements distribution by means of energy dispersive X-ray microanalysis.

Thermal diffusivity was measured using the laser flash technique with a FlashLine 5000 Anter Corporation instrument. Measurements were done in vacuum in a temperature range from 300 to 773 K. The technique involves the deposition of heat via a laser pulse on one face of a thin disk specimen and the recording of the

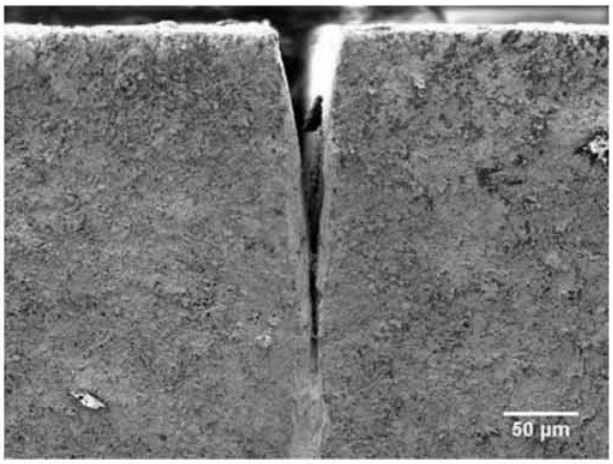

Fig. 1. Scanning electron micrograph of a W−5Ta fracture toughness sample with femtosecond laser notch.

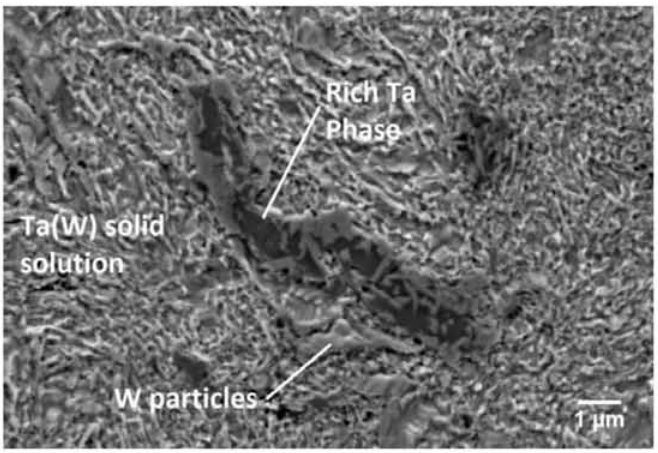

Fig. 2. Scanning electron micrograph of a W−5Ta sample after etching with Murakami reagent. EDS analysis revealed that dark grey particles correspond to Ta pools, observing the diffusion of W from the Ta(W) solid solution.

temperature rise on the other face. Thermal diffusivity is then derived from the time dependence of the measured temperature rise. The apparatus consists of a pulsed laser energy source, a vacuum oven for heating the test specimens, and a data acquisition system [13].

3. Results and discussion

3.1. Microstructure

Secondary electron images and Energy-dispersive X-ray spectroscopymaps of the sintered materials are presented in Figs. 2 and 3. The study of W−5Ta microstructure via metallography and etching with Murakami reagent shows three different phases: i) lagoons of tantalum, ii) large tungsten grains, and iii) Ta(W) solid solution surrounding the W grains, as shown in Fig. 2.

Due to the long milling time during manufacturing, around 50 h, nanometric grains were produced and are difficult to appreciate in SEM images. Nevertheless, as observed in the fractographical analysis (shown in Figs. 8 and 9) the faceted fracture surfaces revealed an average grain size of 50 nm for this Ta(W) phase with coarser grains of W and Ta over several microns. These heterogeneities may stem from the inner core of the powder particles after MA, revealing that although a very effective partial reduction in particle size was observed, the system had not yet achieved steady-state.

In contrast to that observed for W−5Ta, two distinct phases (distinguishable by colour/pattern contrast) can be identified from the backscattered SEM images of the W−15Ta composite presented in Fig. 3. The EDS map confirms that the grey-pattern phase and the solid phase are that of a W-rich phase and a Ta-rich phase, respectively, both composed of smaller grains, with average sizes smaller than 30 µm. This observation can be better appreciated in the fractographical analysis presented in Figs. 10 and 11.

3.2. Mechanical properties

Table 1 summarizes materials densities: experimental, theoretical and relative, as well as the calculated porosity. Densification was determined to lie between 91.81% of the theoretical value for W−5Ta and 92.96% for W−15Ta, whilst the relative density of

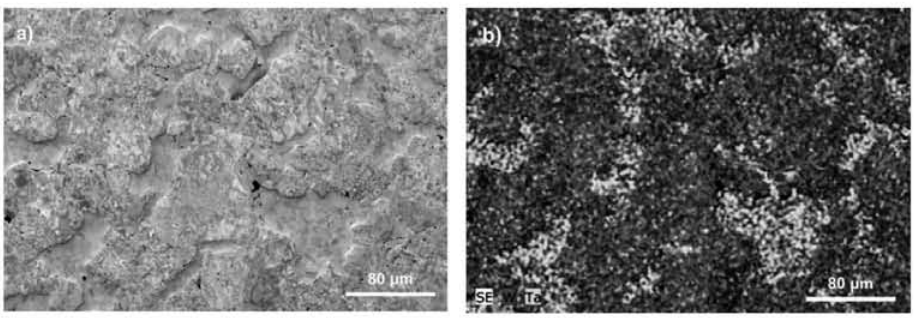

Fig. 3. Scanning electron micrograph of a polished section of W−15Ta showing size and distribution of W and Ta phases. (a) Secondary electrons image. (b) EDS mapping of W (red) and Ta (green) in (a). The dark spots correspond to porosity (For interpretation of the references to colour in this figure legend, the reader is referred to the web version of this article).

Table 1
Density of reference pure tungsten, W−5Ta and W−15Ta materials.

Alloy	Experimental (g/cm^3)	Theoretical (g/cm^3)	Relative (%)	Porosity (%)
Pure W [10]	17.64 ± 0.02	19.25	91.64	8.36
W−5 wt. % Ta	17.54 ± 0.01	19.10	91.81	8.19
W−15 wt. % Ta	17.49 ± 0.12	18.82	92.96	7.04

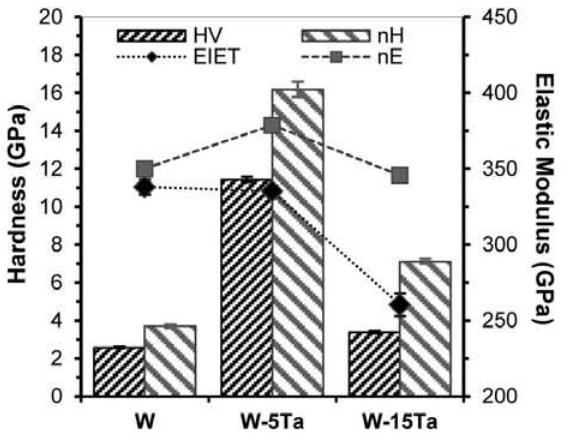

Fig. 4. Vickers micro-hardness (HV), Berkovich instrumented nano-indentation hardness (nH), elastic modulus measured with the impulse excitation technique (EIET) and elastic modulus from nano-indentation tests (nE) for pure W, W–5Ta and W–15Ta.

reference pure tungsten was 91.64%. This indicates an increase in the densification with Ta content, even after an extended milling time for W–5Ta material. In consequence, no clear correlation of the densification after HIP with the manufacturing conditions can be deduced from these results. Nevertheless, porosity could be attributed to the Kirkendall effect, as the maximum temperature reached during the HIP process was 1573 K, which represents only 0.43 T_{hom} for Ta and just 0.39 T_{hom} for W.

At the same time, the measured hardness, HV and nH (Fig. 4) significantly increases from pure tungsten to W–Ta materials, being three times higher in the case of W–5Ta. This indicates an increase in mechanical strength but also of brittleness with the addition of 5 wt. % Ta, as will be confirmed later on (Fig. 5). On the other hand, W–15Ta exhibits approximately twice the hardness of pure W, hence is significantly lower than W–5Ta. This difference

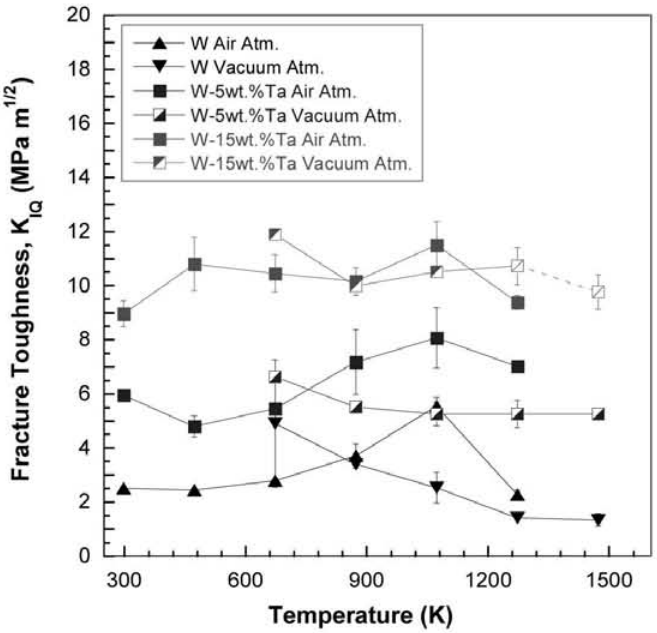

Fig. 5. Nominal fracture toughness of W–5Ta, W–15Ta and pure tungsten alloys tested as a function of temperature. The error bars correspond to the standard deviation of the experimental data.

could be attributed to the difference values of hardness of pure Ta and pure W, but mainly to their microstructure.

Furthermore, results obtained after micro-indentation tests can be correlated with microstructure, and grain size diameter, d, according to the Hall-Petch (HP) relation [14,15]. The HP equation establishes that yield strength varies with $d^{-0.5}$ in a number of metals and alloys, including tungsten [16]. Similarly, it was reported that the HP equation can successfully describe the effect of grain size on hardness [17]. The difference between the grain sizes of the materials tested, 50 nm for W–5Ta and 30 μm for W–15Ta, can justify the VH values obtained. Additionally, this variance in grain size and therefore in grain boundaries, possibly affects nanohardness due to the dislocations interacting with the grain boundaries as they move. The nH values are slightly higher than the ones obtained by micro-indentation, but this variance is attributed to the different definition of hardness for both tests: projected contact area versus indenter contact area, for nH and HV, respectively.

On the other hand, when analysing elastic modulus, it was not easy to identify clear tendencies due to the important influence of porosity on elastic modulus but also of phases and grains sizes. Nevertheless, the values exhibit the order of magnitude expected for tungsten alloys.

3.2.1. Fracture toughness

The variation of fracture toughness with temperature for the two materials tested is shown in Fig. 5. As K_{IQ} loses validity with increasing ductile behaviour, the calculated values above the transition regime give only a lower bound and are denoted by open symbols.

At all temperatures, both in air and vacuum, the fracture toughness increases with increasing Ta content. However the increase in fracture toughness with temperature is significantly higher (over 3.5 times higher than the reference W at RT) for W–15Ta even at the highest temperatures tested. Those values are in reasonably good agreement with data reported in the literature [18] for tests conducted on W–Ta alloys of nominally 1, 5 and 10 wt. % of tantalum. Even while their investigations were carried out on forged specimens, similar conclusions are reached when considering samples with the crack plane parallel to the forging direction. Those authors also reported the increase in fracture toughness with temperature, until a change in fracture behaviour and a drop in global fracture toughness was observed. This maximum value of K_{IQ} can also be observed in Fig. 5 at 1073 K and was explained [19] as the onset of yielding, i.e. BDTT of the intergranular fracture mode. At low temperatures, specimens fail by brittle fracture with cracks propagating easily through the grain boundaries. On the other hand, at higher temperatures, materials are ductile so that only blunting of the notch tip occurs. This effect is also more visible in air experiments, where the oxides on the surface of the notch could lead to unrealistic higher K_{iQ} values.

3.2.2. Flexural strength

The TPB testing produced load–displacement data spanning a temperature range of 298–1273 K in air and 673–1473 K in an inert/vacuum atmosphere. These data have been converted to stress–strain and are presented in Fig. 6 for both materials. Furthermore, ultimate flexural strength values have been summarized and are presented in Fig. 7 as a function of temperature.

As opposed to the observations for fracture toughness, the W–5Ta alloy exhibits a significantly higher strength as well as a higher DBTT – around 1373 K – than the W–15Ta material. The W–5Ta specimens failed by brittle fracture at low temperatures and the transition from brittle to ductile fracture behaviour can be observed with increasing temperature, marked by a steep increase

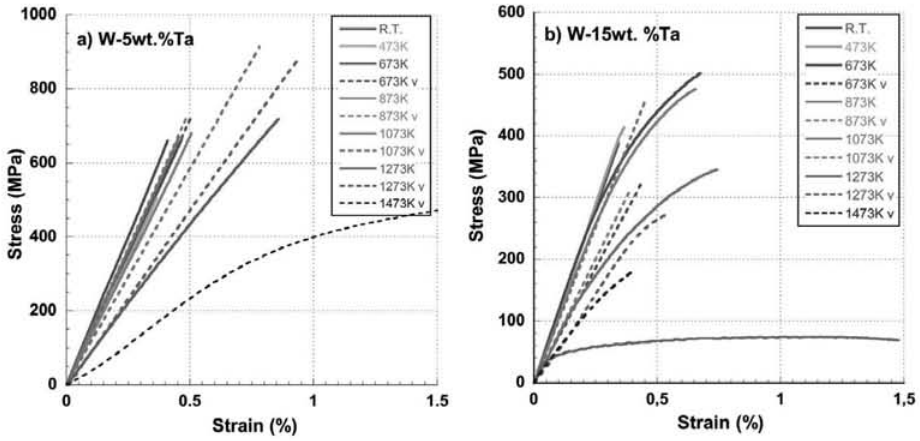

Fig. 6. Stress–strain curves from non-standard three-point bending tests on: a) W–5Ta and b) W–15Ta at different temperatures. Dashed lines represent tests performed in vacuum atmosphere.

of flexural strength at 1373 K. Up to this temperature, the degradation of the material is visible even under vacuum atmosphere, probably owing to the porosity decreasing the alloy cohesion.

Whilst this alloy has a very abrupt DBTT in the range 1273–1373 K, W–15Ta exhibits a smooth transition from brittle to ductile fracture, starting at about 673 K in vacuum but being fully visible over 1073 K. Moreover, although the average ultimate flexural strength of this alloy is approximately 1.5 times lower than that observed for W–5Ta (but almost twice as high than for the reference W), the effect of the atmosphere is less detrimental, as its behaviour is similar up to 1273 K when the material is thoroughly oxidized. In view of this data, we could establish that the increase in Ta content may inhibit the oxidation of W.

3.2.3. *Fractographical analysis*

The dominant failure mechanisms at ambient temperature were similar in both materials: intergranular cracking as well as fracture by cleavage of microstructural heterogeneities, i.e. large W and Ta grains, especially for W–5Ta (Figs. 8 and 9).

As a result of the sub-granular structure of the W–5Ta alloy, with grains smaller than 50 nm, many small facets can be observed on the fracture surface. Moreover, partially pulled-out grains could be regularly found, as well as the presence of many small pores mainly on the grain boundaries. These brittle fracture mechanisms are responsible for the low toughness of the materials as shown in Fig. 5.

Additionally, Fig. 9 of a post-mortem specimen illustrates that W particles of similar size tend to bring into line in a precise way. The influence on the mechanical properties and on the DBTT of W–5Ta has being previously reported with commercial forged materials [20]. Those tests also reported an intergranular fracture mode in this system, with the crack propagating straight through the sample and failing in a brittle intergranular manner.

As opposed to observations for W–5Ta, W–15Ta specimens show a much greater amount of trans-crystalline fracture and plastic deformation of grain boundaries (see Figs. 10 and 11), especially at high temperatures. Therefore, the amount of trans-crystalline fracture seems to be correlated with the fracture

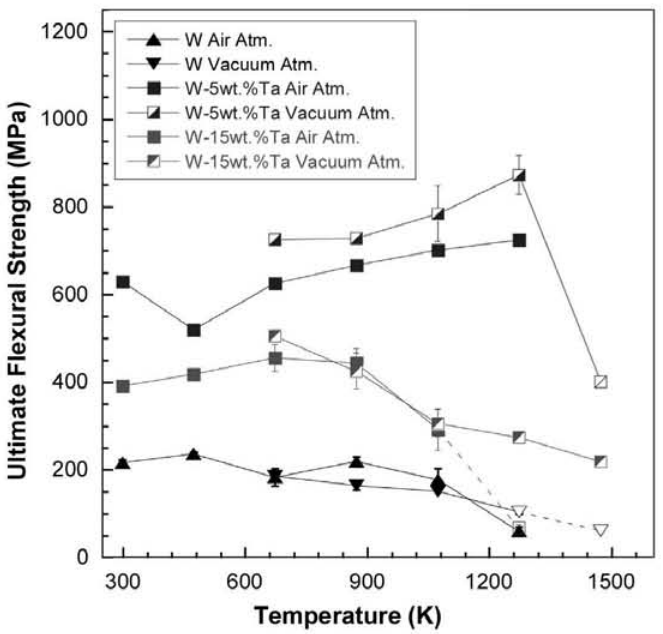

Fig. 7. Ultimate flexural strength versus test temperature for W–5Ta, W–15Ta and pure tungsten in air and vacuum. The open symbols and dashed lines represent the yield strength at 0.2% when the materials exhibited a ductile behaviour.

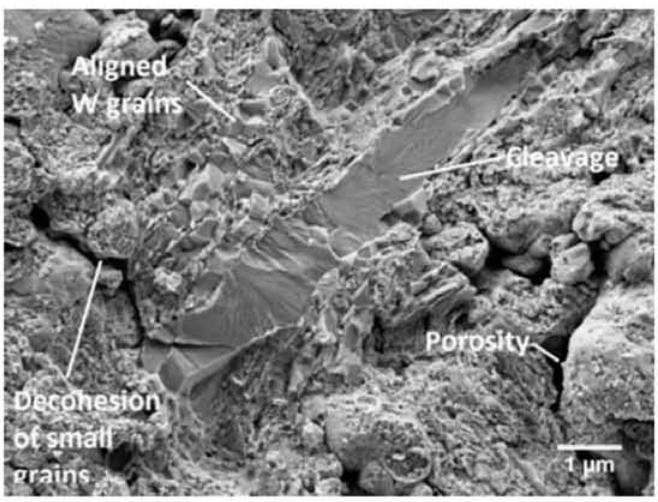

Fig. 8. Fractograph of W–5Ta specimen tested at room temperature. As the grains possess subgrains with a size smaller than 1 μm, the micrographs show strongly facetted fracture surfaces, cleavage of coarse grains, aligned W grains and visible porosity.

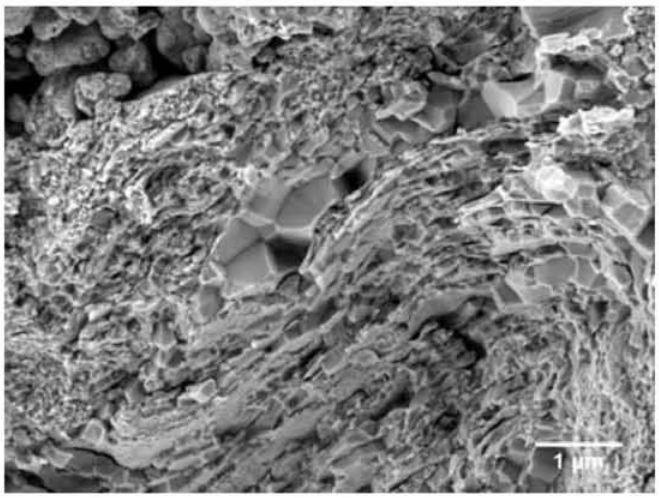

Fig. 9. Fractograph of W–5 wt. % Ta specimen tested at room temperature.

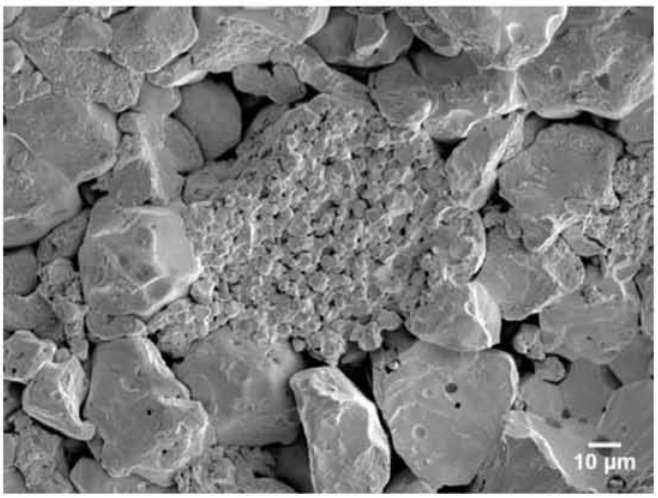

Fig. 11. Fractograph of W–15 wt. % Ta specimen tested at room temperature.

toughness of the samples, as K_{IQ} is about twice as high. For this material, the crack is triggered within the large and linked-up W/Ta regions as it cannot propagate easily over long distances within the more brittle phase.

In addition to the fracture behaviour, fractography analysis also revealed the presence of nanometric grains, but stick together into larger conglomerates of nearly 100 μm (Fig. 11).

3.3. Thermal diffusivity

The change in thermal diffusivity for the W–Ta materials with temperature is shown in Fig. 12. Due to the lack of results for our pure tungsten reference material, those have been compared with two different pure tungsten products: W-UHP, ultra-high-purity tungsten (99.9999 wt. %) [21] and a commercial tungsten grade [22] processed by the same powder metallurgy route as our materials. M. Wirtz et al. [21] also tested a commercial W–5Ta product; hence their values have also been used as a reference.

For all the materials exposed, thermal diffusivity decreased with an increase of test temperature, especially below 600 K; up to this temperature, the gradient is less pronounced. The thermal diffusivity of W–5Ta and W–15Ta materials is similar, however lower than for pure tungsten as observed in Fig. 12 and in the same range of what has been measured for W–Re alloys [23]. The theoretical density of two alloys is similar (91,81 for W–5Ta and 92,96 for W–15Ta) which suggests that residual porosity has a stronger influence on the conductivity of the composite materials than Ta content.

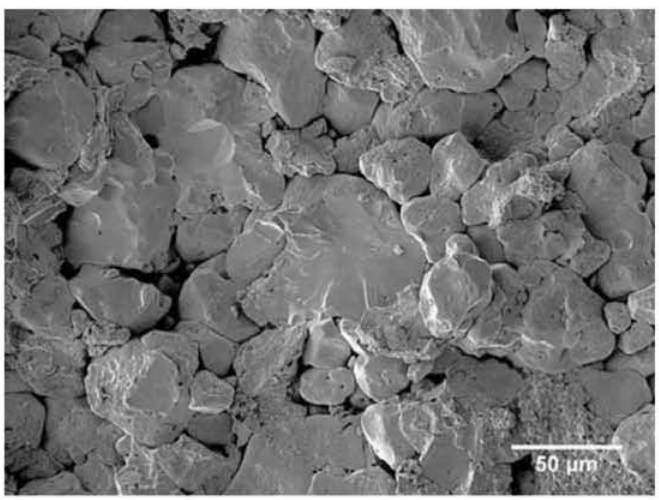

Fig. 10. Fracture surface of W–15Ta tested at 1473 K in vacuum atmosphere showing intergranular fracture and cleavage of W grains.

4. Conclusions

Two W–Ta materials were manufactured by hot isostatic pressing using standard powder metallurgy techniques. After HIPing a density around 92% was achieved for both systems. A very fine microstructure, consisting of grains of Ta(W) solid solution in the submicron range, surrounding Ta pools and non-milled W grains, was found in the case of W–5Ta. By contrast, the W–15Ta material presented a biphasic microstructure composed of both W-rich and Ta-rich phases.

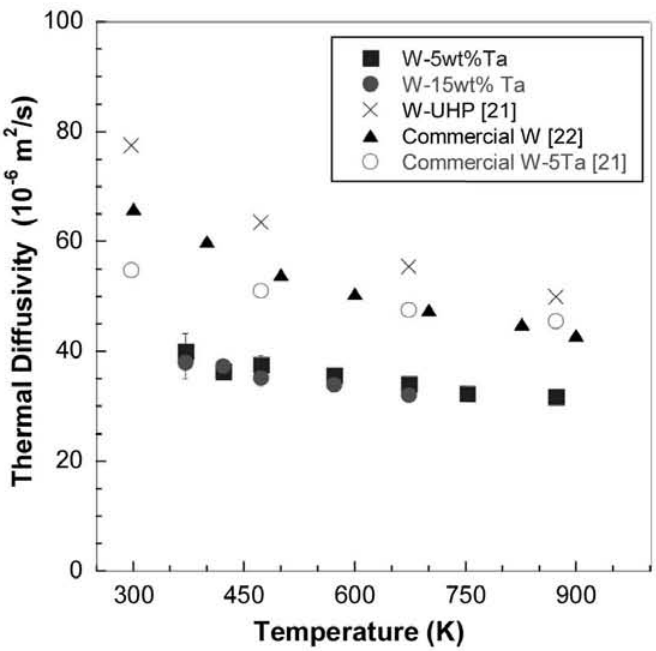

Fig. 12. Evolution of thermal diffusivity with temperature for W–5Ta and W–15Ta. Those results have been compared with referenced materials: commercial W–5Ta and pure W and W-UHP.

Their mechanical properties (strength and toughness) were measured by means of three-point bending tests on smooth and notched specimens from 300 K up to 1273 K in air and to 1473 K in high vacuum. The thermal and mechanical properties of the W–5Ta material are dominated by the refined microstructure; it shows a sharp ductile-to-brittle transition in the range 1273–1323 K but, by contrast, with very poor fracture toughness, due to decohesion of those small grains. This average grain size is also responsible for the high hardness exhibited by this material.

In the case of the W–15Ta system, the thermal conductivity is close to 32 mm^2/s at the maximum temperature tested, 673 K, indeed lower than the literature references, but quite similar to that observed for the W–5Ta material. However, it exhibits significantly higher fracture toughness and lower DBTT – around 673 K – than the W–5Ta material. Therefore, the improvement in toughness of the W–15Ta system could be attributed to a change in the fracture initiation mechanisms, as the DBTT of this material is lower.

To conclude, it has been determined that the addition of Ta enhances the mechanical performance of pure W, although it has a detrimental effect on the DBTT, more patent with lower percentages of Ta. Nevertheless, a possible way to solve this issue has been proposed [24,25] for other tungsten alloys, consisting of the performance of a thermo-mechanical treatment at higher temperatures. Further investigations into the effect of milling time and chemistry are currently on-going, but it appears that tantalum has no beneficial effects on the DBTT of tungsten after the proposed milling-HIP processing.

Acknowledgements

This work has been carried out within the framework of the EUROfusion Consortium and has received funding from the Euratom research and training program 2014–2018 under grant agreement No 633053. The views and opinions expressed herein do not necessarily reflect those of the European Commission. In addition, research by E. Tejado was supported by the CSIC (JAE-Predoc program) co-financed by FSE supports. The authors would also like to acknowledge the Ministerio de Economía y Competitividad of Spain for funding for the research project MAT2012-38541-C02-02 and Comunidad de Madrid (research project S2013/MIT-2862-MULTIMATCHALLENGE).

References

[1] V. Borovikov, et al., Possible Self-healing in Tungsten under Fusion Reactor Conditions, ADTSC Science Highlights, Los Alamos National Laboratory, 2012.
J.W. Davis, V.R. Barabash, A. Makhankov, L. Plöchl, K.T. Slattery, Assessment of tungsten for use in the ITER plasma facing components1, J. Nucl. Mater. 258–263 (Part 1) (1998) 308–312.
W.D. Klopp, A review of chromium, molybdenum and tungsten alloys, J. Less Common Met. 42 (1975) 261–278.
Y. Mutoh, K. Ichikawa, K. Nagata, M. Takeuchi, J. Mater. Sci. 30 (1995) 770–775.
K. Hesch, J. Aktaa, S. Antusch, L.V. Boccaccini, C. Day, D. Demange, W. Fietz, G. Gantenbein, A. Möslang, P. Norajitra, M. Rieth, Technology developments at KIT towards a magnetic confinement fusion power plant, Trans. Fusion Sci. Technol. 61 (2012) S.64–69.
N. Baluc, et al., Nucl. Fusion 47 (2007) S696–S717.
M.R. Gilbert, J.-Ch. Sublet, Neutron-induced transmutation effects in W and W-alloys in a fusion environment, Nucl. Fusion 51 (2011) 043005.
G.A. Cottrell, R. Kemp, H.K.D.H. Bhadeshia, G.R. Odette, T.J. Yamamoto, J. Nucl. Mater. 367–370 (2007) 603–609.
M. Dias, F. Guerreiro, J.B. Guerreiro, A. Galatanu, M. Rosinski, M.A. Monge, E. Alves, P.A. Carvalho, Consolidation of W-Ta Composites: Hot Isostatic Pressing and Spark and Pulse Plasma Sintering, submitted in SOFT conference, 2014.
T. Palacios, A. Jiménez, A. Muñoz, M.A. Monge, C. Ballesteros, J.Y. Pastor, Mechanical characterisation of tungsten–1 wt.% yttrium oxide as a function of temperature and atmosphere, J. Nucl. Mater. 454 (1–3) (2014) 455–461.
W.C. Oliver, G.M. Pharr, An improved technique for determining hardness and elastic modulus using load and displacement sensing indentation experiments, J. Mater. Res. 7 (6) (1992).
G.V. Guinea, J.Y. Pastor, J. Planas, M. Elices, Stress intensity factor, compliance and CMOD for a general three-point-bend beam, Int. J. Fract. 83 (1998) 103–116.
B.N. Enweani, J.W. Davis, A.A. Haasz, Thermal diffusivity/conductivity of doped graphites, J. Nucl. Mater. 224 (1995) 245–253.
E.O. Hall, Proc. R. Soc. B 64 (1951) 747.
N.J. Petch, J. Iron Steel Inst. 174 (1953) 25.
U.K. Vashi, R.W. Armstrong, G.E. Zima, Metall. Trans. 1 (1970) 1769–1771.
R.W. Armstrong, Metall. Trans. 1 (1970) 1169.
S. Wurster, B. Gludovatz, A. Hoffmann, R. Pippan, Fracture behaviour of tungsten–vanadium and tungsten–tantalum alloys and composites, J. Nucl. Mater. 413 (3) (2011) 166–176.
D. Rupp, S.M. Weygand, Anisotropic fracture behaviour and brittle-to-ductile transition of polycrystalline tungsten, Philos. Mag. 90 (30) (2010) 4055–4069.
M. Rieth, S.L. Dudarev, et al., Recent progress in research on tungsten materials for nuclear fusion applications in Europe, J. Nucl. Mater. 432 (1–3) (January 2013) 482–500. ISSN 0022–3115.
M. Wirtz, et al., Comparison of the thermal shock performance of different tungsten grades and the influence of microstructure on the damage behaviour, Phys. Scr. 2011 (2011) 014058.
Y.S. Touloukian, R.W. Powell, C.Y. Ho, M.C. Nicolaou, Thermophys. Prop. Matter 10 (1973). Thermal Diffusivity, IFI/Plenum.
R. Eck, E. Pink, Refract. Met. Hard Mater. 11 (1992) 337.
P. López-Ruiz, N. Ordás, I. Iturriza, M. Walter, E. Gaganidze, S. Lindig, F. Koch, C. García-Rosales, Powder metallurgical processing of self-passivating tungsten alloys for fusion first wall application, J. Nucl. Mater. 442 (1–3, Suppl. 1) (November 2013) S219–S224.
M. Fujitsuka, B. Tsuchiya, I. Mutoh, T. Tanabe, T. Shikama, J. Nucl. Mater. 283–287 (Part 2) (December 2000) 1148–1151.